Fault tolerance in parity-state linear optical quantum computing

A. J. F. Hayes,[1,*] H. L. Haselgrove,[2] Alexei Gilchrist,[3] and T. C. Ralph[1]

[1]*Centre for Quantum Computer Technology and Physics Department, University of Queensland, QLD 4072, Brisbane, Australia*
[2]*C3I Division, Defence Science and Technology Organisation, Canberra, ACT 2600, Australia*
[3]*Physics Department, Macquarie University, Sydney, NSW 2109, Australia*

We use a combination of analytical and numerical techniques to calculate the noise threshold and resource requirements for a linear optical quantum computing scheme based on parity-state encoding. Parity-state encoding is used at the lowest level of code concatenation in order to efficiently correct errors arising from the inherent nondeterminism of two-qubit linear-optical gates. When combined with teleported error-correction (using either a Steane or Golay code) at higher levels of concatenation, the parity-state scheme is found to achieve a saving of approximately three orders of magnitude in resources when compared to the cluster state scheme, at a cost of a somewhat reduced noise threshold.

PACS number(s): 03.67.Pp, 03.67.Lx, 42.50.Ex

I. INTRODUCTION

It was shown by Knill, Laflame, and Milburn (KLM) [1] that, in principle, scalable optical quantum computing could be achieved using only passive linear elements, single-photon sources, measurement, and feedforward. Nondeterministic gates were developed that failed through the accidental measurement of qubit value. Parity-state error codes were developed to protect against such accidental measurement. KLM showed that, by concatenating the parity codes, gate failures could be reduced to arbitrarily small levels, thus justifying the claim of scalibility. However, because of the massive complexity of the scheme, it has not been practical to couple it to a higher-level error correction protocol capable of correcting environmental errors and hence evaluate its resource requirements and fault-tolerant threshold.

A major simplification of the KLM circuit approach was achieved by the introduction of incremental parity codes [2] and fusion gate techniques [3,4]. We refer to this modification of KLM as parity-state quantum computing. These techniques reduce the complexity of the scheme sufficiently that it becomes possible to make a full fault tolerant analysis, thus completing the original KLM program.

In this article, we derive the resource usage and error thresholds achievable when a concatenated error-correcting code such as the STEANE code [5] is used to to handle environmental and residual gate errors in the parity-state optical quantum computing scheme. This type of analysis has previously been done for cluster state [6] and cat state [7] (also known as coherent state) schemes. It is important to establish these thresholds for the parity-state implementation both as a target for technological development and for comparison with the other proposals. Our results show that the parity-state protocol may offer a useful trade-off between the higher resource usage of cluster-state schemes and the lower noise threshold of cat state schemes.

Significant progress has been made in optical quantum computing experiments in the last decade [8]. In particular the basic principles of optical parity-state production and their ability to

correct Z-measurement errors has been demonstrated [9–11]. These promising experiments indicate that effective use of such error-correcting codes in future designs is viable.

The layout of the article as follows. Section II gives a brief review and introduction of parity encoding and the operations that may be done on parity-encoded states. Section III describes the physical noise model that we consider and gives expressions for the effective noise rates on various parity-encoded operations. In Sec. IV these error-rate expressions are used as the basis of simulations of higher levels of encoding. The results of the simulations are presented in the form of noise-threshold curves. Finally, Sec. V considers the resources required by this scheme and provides a comparison with the thresholds and resource requirements of some other schemes for fault-tolerant optical quantum computation.

II. UNIVERSAL GATE SET

This section describes the states and operations used in the two lowest levels of encoding in our scheme: the physical qubits in the dual-rail nondeterministic linear-optical architecture and the first level of logical qubits which use parity-state encoding. These designs lead to the central focus of this article, a discussion of the effects of noise on the parity-state encoding and the effects of higher levels of encoding (fault-tolerant STEANE and GOLAY encoding), which is covered in Secs. III–V.

A. Physical encoding and operations

At the physical level, qubits in our scheme are encoded and manipulated according to the techniques of nondeterministic dual-rail linear optics. Although other implementations, such as spatial encoding, are possible, we will explicitly consider polarization qubits, encoded in the horizontal and vertical polarization modes of single photons. This entails a series of physical and technological assumptions including the following: that single-photon states can be produced on-demand in a desired mode, such modes can be made to interact using mode-matched linear optics, modes can be stored in a quantum memory, and the number of photons in a mode can be measured and the results used in the fast control of
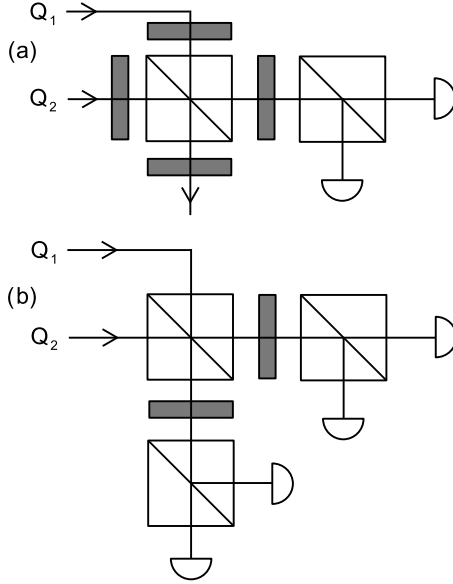
---

*ahayes@physics.uq.edu.au

FIG. 1. (a) The type I fusion gate. (b) The type II fusion gate. Here the gates are shown being performed on two polarization-encoded photonic input qubits, Q_1 and Q_2. These input qubits are typically part of larger entangled states. The gates are constructed from photon-counting detectors, polarizing beam-splitters, and half-wave plates, where the half-wave plates act as Hadamard operations on the polarization qubits.

optical switching. Single-qubit operations in this scheme are relatively straightforward, but two-qubit gates are inherently nondeterministic even in the absence of noise.

As in Ref. [3], our scheme utilizes two particularly simple nondeterministic two-qubit gates, the so-called type I (f_I) and type II (f_{II}) fusion gates (Fig. 1). A type II fusion gate performs a two-qubit destructive measurement in the basis $\{|00\rangle + |11\rangle, |00\rangle - |11\rangle, |01\rangle, |10\rangle\}$. The first two outcomes (corresponding to maximally entangled basis elements) are considered "successful," whereas the second two outcomes are considered to be failures of the gate. A type I fusion gate is a partial Bell measurement on two qubits. Two outcomes, considered successful, project the input state into the space spanned by $\{|00\rangle, |11\rangle\}$ and outputs a single qubit according to the operator $|0\rangle\langle00| \pm |1\rangle\langle11|$. Again, there are two failure outcomes which correspond to a destructive measurement in the basis $\{|01\rangle, |10\rangle\}$.

For the type of input states we will consider, both the type I and type II fusion gates are successful with 50% probability (in the absence of noise).

B. Parity encoding

A length-n *parity code* encodes one logical qubit into n physical qubits. The logical basis states of the code, denoted $|0\rangle^{(n)}$ and $|1\rangle^{(n)}$, are defined to be:

$$|0\rangle^{(n)} \equiv (|+\rangle^{\otimes n} + |-\rangle^{\otimes n})/\sqrt{2}$$
$$|1\rangle^{(n)} \equiv (|+\rangle^{\otimes n} - |-\rangle^{\otimes n})/\sqrt{2}, \quad (1)$$

where $|\pm\rangle = (|0\rangle \pm |1\rangle)/\sqrt{2}$. Note that $|0\rangle^{(n)}$ is the equal superposition of all even-parity n-bit strings and $|1\rangle^{(n)}$ is the equal superposition of all odd-parity strings. A useful property

of the parity-code basis states is that they have a simple expansion in terms of smaller code states:

$$|0\rangle^{(n)} = (|0\rangle^{(n-j)}|0\rangle^{(j)} + |1\rangle^{(n-j)}|1\rangle^{(j)})/\sqrt{2}, \quad (2)$$
$$|1\rangle^{(n)} = (|1\rangle^{(n-j)}|0\rangle^{(j)} + |0\rangle^{(n-j)}|1\rangle^{(j)})/\sqrt{2}, \quad (3)$$

where $1 \leqslant j \leqslant n - 1$. For $j = 1$ this expansion shows that a computational basis measurement (such as occurs with a failed fusion gate) of one of the physical qubits will not destroy a parity-encoded qubit, but will only reduce the length of encoding by 1 (and possibly introduce a known logical Pauli X operation, depending on the measurement outcome).

C. Generating parity states

The production of parity-encoded states is a necessary procedure both for the preparation of encoded qubits as sources and as part of the resource generation required by some of the nondeterministic logical gates in our universal gate set for parity-encoded qubits.

The state $|0\rangle^{(n)}$ is locally equivalent to a star-shaped cluster state (by a Hadamard operation applied to the central node of the star). Consequently, given a supply of Bell states ($|0\rangle^{(2)}$), the resource $|0\rangle^{(n)}$ can be built up using essentially the same techniques as used in [3] to build up star-shaped cluster states.

Parity states $|0\rangle^{(n)}$ and $|0\rangle^{(m)}$ can be *fused* using the f_I gate as follows:

$$H f_I(H \otimes H)|0\rangle^{(n)}|0\rangle^{(m)} \rightarrow \begin{cases} |0\rangle^{(m+n-1)} & \text{(success)} \\ |+\rangle^{\otimes n-1}|-\rangle^{\otimes m-1} & \text{(failure)} \end{cases} \quad (4)$$

(where we have omitted other possible locally equivalent outcomes for both success and failure). The operator $H f_I(H \otimes H)$ should be understood as a Hadamard gate acting on one of the physical qubits from each of the encoded states, followed by the f_I gate applied to the same pair, followed by a Hadamard gate applied to the output of f_I in the case of success. Alternatively the f_{II} gate can be used to carry out fusion, as follows:

$$f_{II}|0\rangle^{(n)}|0\rangle^{(m)} \rightarrow \begin{cases} |0\rangle^{(m+n-2)} & \text{(success)} \\ |0\rangle^{(m-1)}|0\rangle^{(n-1)} & \text{(failure)} \end{cases} \quad (5)$$

(again, some additional locally equivalent outcomes have been omitted).

The first alternative, where f_I is used with Hadamard gates to perform fusion, has the advantage of losing only a single physical qubit from the input states, but the disadvantage of completely destroying the entanglement in both input states in the event of failure. In the second case, f_{II} is used to join the input states at the expense of losing two of the initial physical qubits. There are three advantages to the second scheme—in the case of failure we do not destroy the entanglement of the input states, just reduce their encoding by 1; we do not need photon number discriminating detectors to operate f_{II}; and it is failsafe with respect to loss, in the sense that a lost photon will not cause a failed f_{II} gate to appear to have operated successfully.

Thus, to create the state $|0\rangle^{(3)}$, two $|0\rangle^{(2)}$ are fused together using the f_I gate. Since f_I functions with a probability of 1/2, on average two attempts are necessary so on average each $|0\rangle^{(3)}$ consumes $4|0\rangle^{(2)}$. Once there is a supply of $|0\rangle^{(3)}$ states, either

f_I or f_{II} can be used to progressively build up larger resource states.

D. Simple single-qubit gates

For the parity code, encoded single-qubit unitaries can be divided into those which have a particulary simple deterministic implementation and those which have a more complicated nondeterministic implementation involving the consumption of resource states.

We can deterministically perform encoded versions of any of the gates in the set $\{X_\theta, Z\}$. Here, X_θ refers to an arbitrary rotation about the x axis of the Bloch sphere, $X_\theta = \cos(\theta/2)I + i\sin(\theta/2)X$. An encoded X_θ operation is achieved by applying X_θ to just one physical qubit in the code state. The encoded Z gate is achieved by applying a Z gate transversally to all physical qubits in the code state.

E. Z_{90} gate

To make our set of encoded single-qubit gates universal, we add the Z_{90} operation. Similarly to the notation introduced in the previous subsection, Z_{90} refers to a rotation by 90° around the z axis of the Bloch sphere.

The logical Z_{90} operation is based on the process of *re-encoding*. Re-encoding can be understood by considering the following generalization of Eq. (5):

$$f_{II}|\Psi\rangle^{(n)}|0\rangle^{(m)} \rightarrow \begin{cases} |\Psi\rangle^{(m+n-2)} & \text{(success)} \\ |\Psi\rangle^{(m-1)}|0\rangle^{(n-1)} & \text{(failure)} \end{cases}, \quad (6)$$

where $|\Psi\rangle^{(n)} \equiv \alpha|0\rangle^{(n)} + \beta|1\rangle^{(n)}$ is an arbitrary parity-encoded input state, and like Eq. (5) we have omitted other locally equivalent outcomes.

To re-encode a logical qubit $|\Psi\rangle^{(n)}$, a type II fusion gate is first performed between the logical qubit and another ancillary parity state $|0\rangle^{(n+1)}$. Then, each of the remaining $n-1$ qubits that belonged to the original encoded input state are measured in the computational basis, leaving the new ancilla qubits in the same state as the original input, $|\Psi\rangle^{(n)}$. A logical X operation may be required as a correction depending on the total parity of the measurements made.

A slight modification of this procedure yields the encoded Z_{90} gate. Let

$$|\Psi\rangle^{(n)} = \alpha(|0\rangle^{(n-1)}|0\rangle_I + |1\rangle^{(n-1)}|1\rangle_I) + \beta(|0\rangle^{(n-1)}|1\rangle_I + |1\rangle^{(n-1)}|0\rangle_I) \quad (7)$$

be the logical qubit on which we wish to perform an encoded Z_{90} operation. One of the component physical qubits (here denoted by the subscript I) is chosen to represent the input for the type II fusion in the re-encoding procedure. To achieve an encoded Z_{90} gate on $|\Psi\rangle^{(n)}$, we simply apply the un-encoded Z_{90} gate to qubit I, then carry out the re-encoding procedure detailed above. The final logical state following a successful fusion is $Z_{90}|\Psi\rangle$. In this case, a correction corresponding to a logical Y operation may need to be applied to the output state depending on the parity of the measurements made. In the event that the fusion gate fails, the size of the input state is reduced, and the operation may be reattempted if there are enough remaining qubits. If all qubits in the input state are depleted, then the logical gate is considered to have failed.
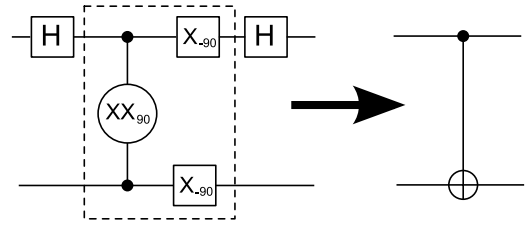

FIG. 2. The relationship between the XX_{90} gate and the controlled-NOT gate. The combined operation inside the dotted area defines the XX'_{90} gate.

To implement a logical Hadamard operation in this gate set we use the decomposition $H = X_{90}Z_{90}X_{90}$. Since operations of the form X_θ are relatively easy to perform, the logical Hadamard is essentially equivalent to the Z_{90} gate in terms of difficulty, time taken, and error emergence.

F. XX'_{90} gate

We define two maximally entangling two-qubit gates XX_{90} and XX'_{90} as follows:

$$XX_{90} \equiv \frac{1}{\sqrt{2}}(I_1 I_2 - i X_1 X_2), \quad (8)$$

$$XX'_{90} \equiv (X_{-90} \otimes X_{-90})XX_{90}. \quad (9)$$

The relationship between the XX_{90}, XX'_{90} and controlled-NOT (CNOT) gates is shown in Fig. 2 in circuit form. XX_{90} and XX'_{90} have the useful property that the parity-encoded versions of these gates can be achieved by applying just one copy of the unencoded gate to a pair of physical qubits (where one physical qubit is selected from each of the encoded input blocks).

An unencoded XX'_{90} can be achieved nondeterministically as follows. First, a four-qubit resource state is created using the circuit shown in Fig. 3. If the three fusion gates are successful,
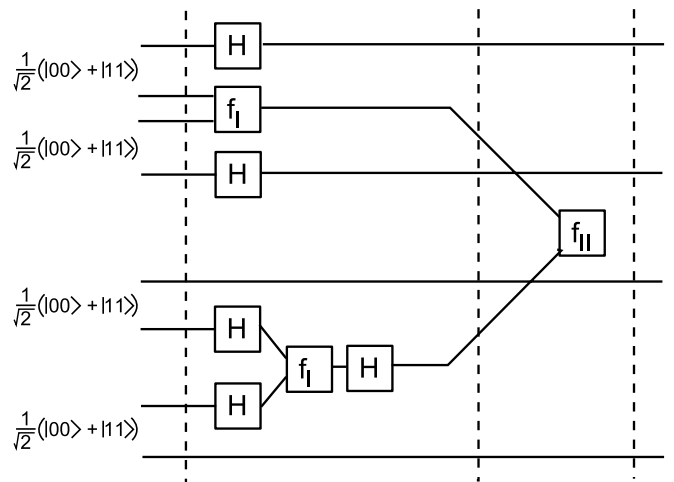

FIG. 3. The circuit used to create the resource state $|R_{XX}\rangle$ used in implementing the XX'_{90} gate. The circuit can be modified by treating the top and bottom qubits as length-2 parity-encoded qubits in order to improve the nondeterministic behavior of the gate.

the resulting state is

$$|R_{XX}\rangle = \tfrac{1}{2}[|++\rangle(|00\rangle+|11\rangle) + |--\rangle(|01\rangle+|10\rangle)].$$
(10)

Next, two f_{II} gates are applied between the input qubits and the resource state in the following manner: a f_{II} gate is applied between a qubit of the first input and the first qubit of the resource state, and a f_{II} gate is applied between a qubit of the second input and the fourth qubit of the resource state. If both are successful, the remaining two qubits will be in the state $XX'_{90}|\psi\rangle$, where $|\psi\rangle$ was the input state (subject to possible known Pauli corrections).

For parity-encoded inputs the procedure is almost identical, except that one has more opportunities to attempt the f_{II} gates between the inputs and the resource state. If both of the f_{II} gates fail, the corresponding encoded input qubits will be reduced in size by 1 and the gate can be reattempted. Note that if one of the f_{II} gates fails and the other succeeds, then one of the input states will be reduced in size by one but the other input effectively retains its size, if we consider one of the remaining qubits in the resource state to now belong to the particular encoded input that corresponds to the fusion gate that succeeded.

The procedure described above provides an encoded XX'_{90} gate which on average decreases the size of its inputs by 1. A simple modification can be made to the resource-state generation circuit so that the resulting gate will instead on average preserve the size of its inputs. The modification involves treating the first and fourth qubits in Fig. 3 as length-2 parity qubits instead of physical qubits, meaning that the resource state is now a state of six physical qubits. We will make use of this version of the XX'_{90} gate in the remainder of the article.

III. ANALYSIS OF ERRORS

A. Error modeling

The theory of error correction in general requires that some assumptions be made concerning the nature of errors that may occur in a system. The set of possible errors that are considered, and their probability, form an error model on which the conclusions of a theory are based. In developing error correction methods, the aim is to choose error models which closely match the physical reality. Typically, this involves focusing on the most common types of error found in the corresponding experimental systems. However, it is not always possible to make the error model a detailed fit to the requirements of a particular system, especially when the technology is still in development.

In optical quantum computing systems with single photons, the greatest source of error is normally photon loss. This can occur in many different ways, including tunneling, detection failure, imperfect coupling, and unreliable sources. Another important type of error in optical systems is dephasing. It is expected that dephasing errors will typically be less frequent than loss errors in future optical computer components but still likely to have a significant effect in any large-scale quantum circuit. These errors can also be caused by imperfect coupling

or, indeed, any misalignment or flaw in the optical elements that can affect the polarization of the photon.

We use a simple error model for the noise on physical qubits. Each gate operation is divided into time steps, with a single time step being roughly the time required to make a measurement or set of measurements and perform feedforward based on the results. Each physical qubit is considered to experience loss at a rate of γ per qubit per time step, and Pauli errors at a rate of η per qubit per time step. The Pauli error is selected randomly from the set $\{X,Y,Z\}$ with equal probability. This corresponds to a depolarization error of rate $\frac{4}{3}\eta$ and to a marginal probability of a bit-flip of $\frac{2}{3}\eta$. Depolarization errors are a generic way of representing the effects of dephasing noise, as well as other errors which act locally on each qubit and do not cause leakage from the qubit state space.

The physical error model described above is used as the basis for estimating the effective error rates on encoded qubits at higher levels of encoding. The relationship between the levels of encoding are summarized in Fig. 4. At each encoding level, the aim is to estimate the rates of two different error types: *located errors*, which are those errors which are heralded (in a way analogous to the failure of fusion gates at the physical encoding level), and *unlocated errors*, which are Pauli errors that are not directly heralded and must be found indirectly via syndrome measurement. The remainder of this section is devoted to deriving expressions approximating the effective error rates of the various parity-encoded operations, i.e., operations at the first level of encoding above the physical level. Then in the following section, these expressions are used as the error model for simulations of concatenated fault-tolerant teleported error correction (*telecorrection*), using STEANE and GOLAY coding.

In deriving expressions for the effective error rates at level 1, we use approximations which are correct only to first order in the physical error rate. In particular, we find the probability that a qubit remains error-free after multiple time steps by taking the product of the individual probabilities of an error not occurring for each time step. In general, this is correct only to first order, since in reality multiple errors of the same type occurring on the same qubit can cancel. For bit- or sign-flip errors of the type included in our error model, an even number of errors has no overall effect on the qubit. However, since we are considering only very small values of physical error rate, and since each parity-encoded gate consists of only a relatively small number of optical components, these higher-order error terms are insignificant.

It is important to note that this model assigns the same error probability to a time step regardless of whether a qubit was involved in operations during that time. Hence this model takes into account errors that arise while a qubit is kept in memory and assumes that such error rates are similar to those for a qubit actively involved in computation. This aspect of the model may be unduly pessimistic, but we have chosen to consider the worst case in this regard.

Having defined the error model, it is also necessary to consider how these errors propagate through the elements of an optical system. First, it should be noted that measurement in the Z basis renders any X errors on that qubit irrelevant (likewise for Z errors and X-basis measurements). Measurement also

1. Telecorrector Circuit

2. Logical CNot Operation

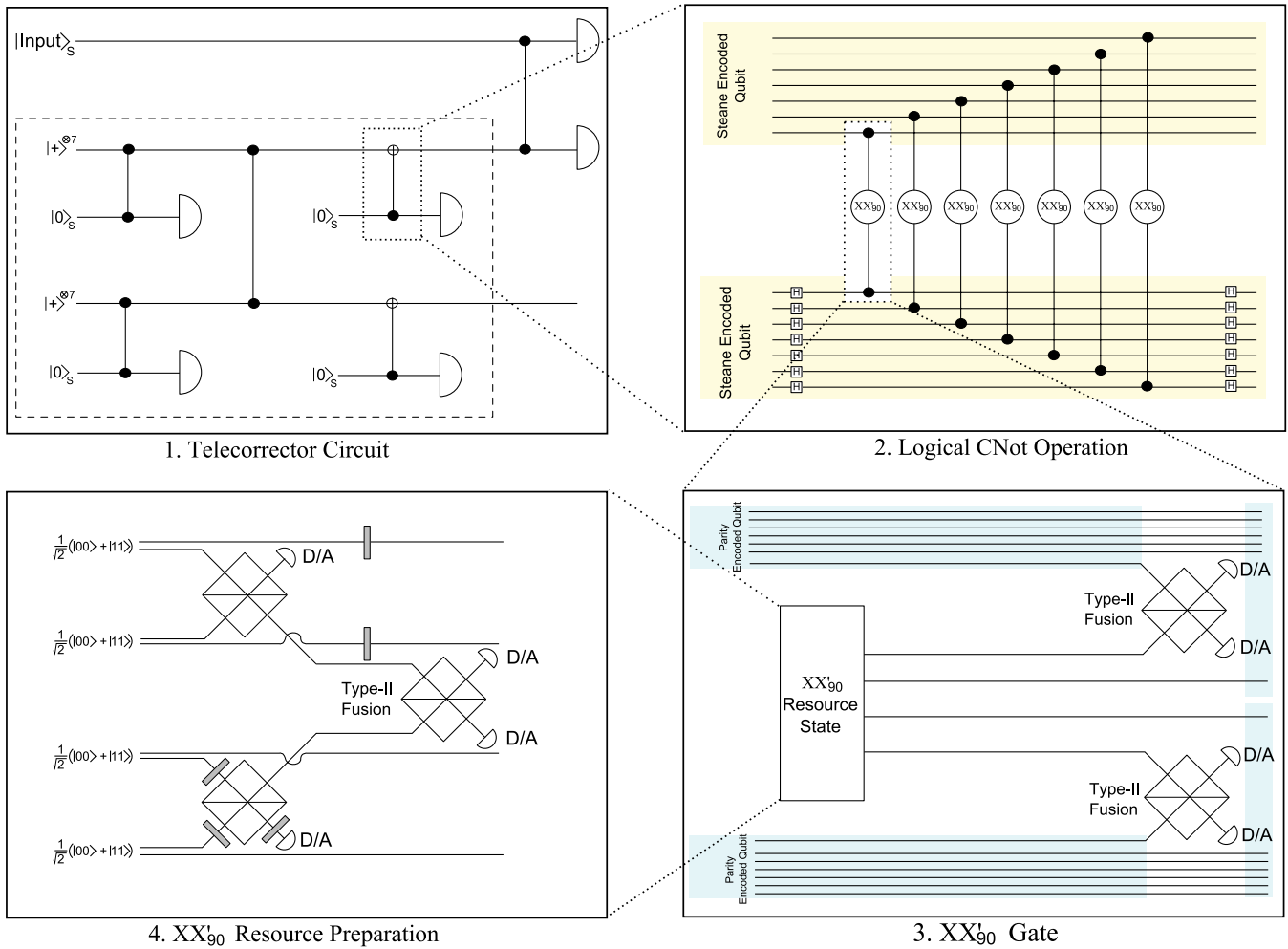4. XX'_{90} Resource Preparation

3. XX'_{90} Gate

FIG. 4. (Color online) The teleported error-corrector (*telecorrector*) circuit shown at different scales. This diagram demonstrates the manner in which logical operations are broken down into a series of operations at the lower layers of encoding. Box 1 shows the circuit for the production of the resource required for one round of telecorrection. Here the subscript "S" indicates qubits encoded using the STEANE code. Box 2 demonstrates how a CNOT gate on the STEANE-encoded qubits can be performed using 7 XX'_{90} gates and 14 Hadamards at the parity encoding layer. Box 3 shows the process of using resource preparation plus teleportation to implement an XX'_{90} gate, and Box 4 provides the circuit used to prepare the required resource.

serves to locate loss errors. Due to the regular measurements that occur in our protocol (either directly or via a fusion gate), it can be seen that loss errors will always be quickly transformed into located errors.

The properties of parity-state encoding are such that any X errors on physical qubits immediately become X errors on the logical, parity-encoded qubit. Hence the probability of a logical X error will depend simply on the rate of such errors at the physical level, the number of qubits, and the duration of the computation. Z errors on individual photonic qubits do not automatically become logical; however, if a photonic qubit on which a Z error has occurred is used as an input for a fusion gate, the error is then applied to all the qubits forming the parity state of which the input qubit was a member. We will use $\eta_X = \eta_Z = \frac{2}{3}\eta$ to denote the marginal error probabilities of X and Z errors (where Y is considered to be "both an X and a Z error"). This notation allows one at a glance to see which physical error type contributes to a particular logical error rate in the expressions of the following subsections.

B. Size of the parity code

There is a trade-off in the located error rate for the nondeterministic gates between the errors due to gate failure and those due to loss (Fig. 5). This occurs as each additional qubit in the encoding increases the possibility of a loss occurring. However, a certain level of encoding is necessary in order to reduce the probability of gate failure. We can optimize the size of the parity states by calculating the located error rates for the nondeterministic operations and examining how these errors vary with code size. Figure 5 shows this relationship for the XX_{90} gate. In this plot, the floor is set at a 10% failure rate as this is the maximum located error rate for which the concatenated STEANE code can drive the error rate arbitrarily close to zero. It can be seen that a seven-qubit encoding offers the best loss threshold for this gate. This also proves to be optimal for the Z_{90} operation.

For loss rates below the threshold, the most efficient parity qubit size for handling located errors will increase, as the intrinsic failure rate of the nondeterministic gates comes to
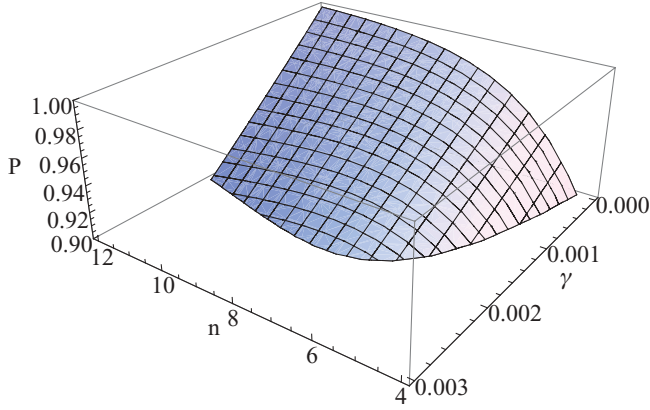
FIG. 5. (Color online) The probability of success for the XX_{90} gate as a function of the photon loss rate (γ) and code size (n).

dominate. Hence it is possible to adjust the code size for greater efficiency if the error rates are known precisely and remain fairly constant. However, it should be noted that a larger parity encoding will also cause an increase in unlocated error rates, which means that smaller codes sizes may still be favored even in a low-loss system. For the purposes of this article, we will solely consider a seven-qubit parity encoding, as this code size gives in the largest range of errors tolerated.

C. Source production

We assume that copies of the state $|0\rangle^{(7)}$ are prepared as needed by massively parallel production in order to have them ready when required by the circuit. We begin with Bell pairs in the state $(|00\rangle + |11\rangle)/\sqrt{2}$ and link these by means of types I and II fusion gates. For a parity state of size 7, seven Bell pairs and six fusion gates are required to build the resource. As each gate has a 50% failure rate, parallel production of each resource requires an average of 7×2^6 Bell pairs and takes three time steps. The resulting state has an unlocated X error rate of $1 - (1 - \eta_X)^{41}$ and a located error rate of $1 - (1 - \gamma)^{21}$. (There are 41 locations in the optical circuit which can contribute errors to the output state. For 20 of these locations, photon loss will be immediately heralded, and so we postselect on no loss occurring at those locations).

D. Z_{90} error rates

This gate occurs in two steps: the first step is the attempt to fuse the encoded state with a resource state, and the second step is measuring the remaining component qubits from the original state once a successful fusion has been performed. The probability of a failure at the first step is:

$$1 - \sum_{j=1}^{7} 2^{-j}(1-\gamma)^{\frac{1}{2}j(1+j)}, \quad (11)$$

which combines the possibility of a loss during fusion with the fusion failure rate to get the total located error rate during fusion attempts. To cover the possibility of loss occurring on any of the other component qubits, we include the factor

$$(1-\gamma)^{3j+(1+j)(7-j)} \quad (12)$$

in the sum, which depends on the number of qubits remaining and the time they have been in memory.

Hence the Z_{90} gate has a combined located error rate per parity qubit of

$$P_{\mathrm{LE}} = 1 - \sum_{j=1}^{7} 2^{-j}(1-\gamma)^{\frac{1}{2}j(1+j)}(1-\gamma)^{3j+(1+j)(7-j)}. \quad (13)$$

For unlocated errors, the average rate can be found by combining the error rates for memory and for producing an ancillary parity state, due to the re-encoding process used to implement the gate. The average time required to implement this gate would be two time steps. However, for all error types, it is assumed that the average time spent is four time steps (this corresponds to the average time required for the slowest gate, XX'_{90}). This is done so that all encoded operation types can be treated as taking an equal amount of time. By counting the number of locations that may contribute to logical errors on the output, we obtain overall effective rates of unlocated X and Z errors of $1 - (1 - \eta_X)^{69}$ and $1 - (1 - \eta_Z)^{10}$ respectively, for the Z_{90} gate.

E. XX_{90} error rates

The propagation of errors through this gate is fairly simple: a Z error on either input qubit will cause an X error on the opposite qubit. X errors on an input qubit propagate to the output without having an effect on the other qubit.

As described in subsection II F, the gate is achieved by performing fusion gates between qubits from the encoded input state and a six-qubit resource state. As we are interested in an error rate per parity qubit, we model the success or failure of the fusion gates applied to an input parity qubit using a random walk on a semi-infinite one-dimensional lattice with 1 absorbing boundary at $-n$ [12]. Here the lattice represents the size of the parity state, with failure occurring either due to a loss or when all component qubits are measured due to repeated teleportation failures.

The number of paths that reach the boundary at time t is

$$N(n,t) = \frac{t!}{(\frac{t+n}{2}!)(\frac{t-n}{2}!)} \quad \text{for } (t-n) \bmod 2 = 0$$
$$N(n,t) = 0 \quad \text{for } (t-n) \bmod 2 = 1, \quad (14)$$

where n is the initial size of the parity code. To incorporate the possibility of a successful gate operation, we include a scaling factor in the number of paths:

$$N_{\mathrm{scaled}}(n,t) = 2^{-\frac{t-n}{2}} N(n,t). \quad (15)$$

The number of first passage paths for this type of walk is

$$F(n,t) = \frac{n}{t} N_{\mathrm{scaled}}(n,t). \quad (16)$$

Therefore, total probability of success per parity qubit in the absence of loss is:

$$P_S = 1 - \sum_{t=n}^{\infty} \frac{F(n,t)}{2^t}. \quad (17)$$

For a parity qubit of size 7, this evaluates to $P_S = 0.9763$.

As the average size of the state and the rate of loss per time step is constant, the average loss per parity qubit during this operation can be simplified to:

$$P_L = 1 - (1-\gamma)^{t(n+3)}. \tag{18}$$

The average time taken for this operation is four time steps. Thus, the approximate located error rate per parity-encoded input is $1 - 0.9763(1-\gamma)^{40}$. The unlocated X and Z error rates, obtained by counting error locations in the average-time case, are $1 - (1-\eta_X)^{28}$ and $1 - (1-\eta_Z)^4$, respectively.

F. Memory and measurement

The memory or identity operation on an encoded qubit simply entails keeping the constituent physical qubits in memory while other operations are performed. We treat the encoded memory operation as taking four time steps, equal to the average time taken to perform the slowest encoded gate, XX'_{90}. This yields approximate rates of X, Z, and located errors of $1 - (1-\eta_X)^{28}$, $1 - (1-\eta_Z)^4$, and $1 - (1-\gamma)^{28}$, respectively.

An encoded computational-basis measurement involves measuring each physical qubit in the computational basis and finding the parity of the measurement results. Thus, the rates of located and unlocated errors in the measurement outcome are $1 - (1-\gamma)^7$ and $1 - (1-\eta_X)^7$, respectively.

IV. FAULT TOLERANCE THRESHOLD

Having analyzed the emergence of logical errors at the parity code layer, we used numerical simulation to calculate the error rates at higher levels of concatenation and, from this, the value of the noise threshold for optical parity-state quantum computation.

The simulations were performed using similar techniques to those described in subsection V D of Ref. [6]. In particular, we simulate one level of the telecorrector protocol for both the 7-qubit (STEANE) and 23-qubit (GOLAY) codes. Our simulation differs from Ref. [6] in the noise model and gate set used. The telecorrector circuit in Ref. [6] uses the following gate set: preparation of $|0\rangle$ and $|+\rangle$ states, CNOT, CPHASE, and X-basis measurement. We converted this circuit to our gate set in the following way. First the circuit was expressed solely in terms of CPHASE gates, Hadamard gates, $|+\rangle$ creation, and X-basis measurements by making appropriate substitutions of each CNOT gate, $|0\rangle$ creation, and computational basis measurements in the circuit and simplifying the resulting circuit where possible. Then a simple change of basis $|0\rangle \leftrightarrow |+\rangle, |1\rangle \leftrightarrow |-\rangle$ yielded a circuit in our gate set (XX'_{90} gates, Hadamard gates, $|0\rangle$ creation, and computational-basis measurement).

We carried out a series of Monte Carlo simulations for a range of values of the physical error rates (γ, η), in each case measuring the resulting rate of unlocated and located errors at the next highest level of encoding. For a particular choice of the physical noise rates, Pauli errors (both unlocated and located) are introduced by each gate with a probability that is governed by the noise model derived in the previous section. In the case of unlocated errors, X and Z errors are introduced independently. For the XX'_{90} gate,

errors are introduced independently on each of the two output qubits.

The results of the simulations were used to characterize the mapping of error rates from the physical level to the second level of encoding (i.e., the parity encoding plus one level of telecorrection encoding) by way of a polynomial fit to the measured values. Let (γ_j, η_j) denote the particular choices of physical error rates for which the simulator was run, and let (Γ_j, H_j) denote the corresponding rates of unlocated and located errors at the second level of encoding as measured by the simulator. We use fitting techniques to find functions $\Gamma(\gamma, \eta)$ and $H(\gamma, \eta)$ which closely approximate the observed values of (Γ_j, H_j) when evaluated at the appropriate values (γ_j, η_j). We perform the polynomial fit so that we have a way of estimating the second-level unlocated and located error rates Γ and H for any arbitrary value of the physical error rates γ and η, even though we have performed the time-consuming simulation step only for some finite set of physical error rates (γ_j, η_j). The order of the polynomials $\Gamma(\gamma, \eta)$ and $H(\gamma, \eta)$ is chosen to be that which results in the mean square error between the polynomials and the data points being roughly equal to the amount of error that is known to be present in the values of (Γ_j, H_j) due to the finite sampling in the Monte Carlo simulations.

We also need a way of estimating error rates at levels of encoding higher than the second. However, the polynomials $\Gamma(\gamma, \eta)$ and $H(\gamma, \eta)$ that we have constructed for mapping error rates from the physical level to the second level are not suitable for mapping from the second to higher levels, since the error correction at higher levels does not include parity encoding. Reference [6] deals with a similar situation, where in their case cluster-state encoding is used only at the lowest level, in analogy with our own use of parity-state encoding. Their solution is to perform a separate set of simulations of a circuit and corresponding noise model that represents a single level of error correction at the third or higher level. Then, from the results of such a simulation they use polynomial fitting to yield polynomials $P(p,q)$ and $Q(p,q)$ which, in analogy with the functions $\Gamma(\gamma, \eta)$ and $H(\gamma, \eta)$ above, map the effective unlocated and located error rates p and q from one level of encoding to the next higher level. The rather generic noise model of unlocated and located errors used by Ref. [6] is applicable to the higher levels of encoding in our situaion too, so we simply take the polynomials $P(p,q)$ and $Q(p,q)$ obtained in Ref. [6] and use them to characterize each of our levels of error correction above the second level. Thus, for a given choice of physical error rates (γ, η), we can estimate the effective error rates at any arbitrary level of encoding by first applying the mapping $(\gamma, \eta) \rightarrow (\Gamma(\gamma, \eta), H(\gamma, \eta))$ and then repeatedly applying the mapping $(p,q) \rightarrow (P(p,q), Q(p,q))$ for as many levels as required.

We say that the physical error rates (γ, η) are *below the noise threshold* if the effective error rates tend to zero in the limit of many levels of encoding. The *threshold curve* is then defined to be the curve in the γ-η plane which separates those values of (γ, η) which are below the noise threshold from those which are not. Calculating the threshold curve simply involves dividing the γ-η plane into a fine grid and testing whether each point is below the threshold by applying the appropriate polynomials some large number of times and then finding the boundary of
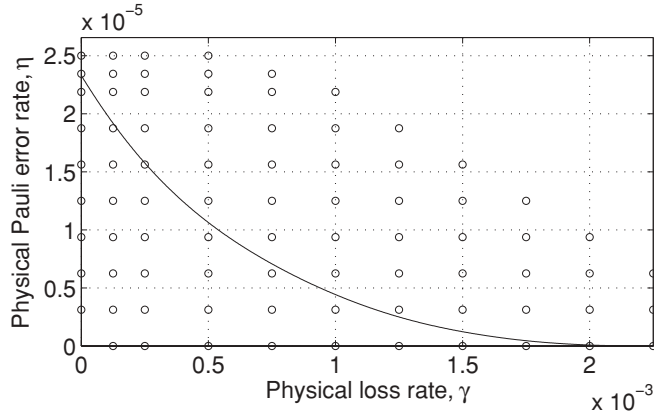
FIG. 6. The threshold curve for optical parity-state computing using the seven-qubit STEANE code. The region below the solid curve represents the set of error rates which can be tolerated by the scheme.

the set of points that were tested to be below the threshold. Our calculated threshold curves are shown in Figs. 6 and 7. In the plots, the small circles show the values of (γ_j, η_j) for which a Monte Carlo simulation was run. (Note that those points are not the same as the much finer grid of points for which the polynomials were evaluated when finding the threshold curve.) Like previous schemes for optical quantum computing, the results demonstrate a trade-off between a tolerance of photon loss and depolarization errors. It is worth noting that the code is always required to deal with some probability of located errors due to the nondeterministic gates and the finite size of the underlying parity encoding. These errors are taken into account when calculating the threshold for the loss and depolarizing rates plotted here.

V. RESOURCES

For a useful comparison with other schemes for error-correcting quantum computing, it is necessary to also consider the resources that would be required to implement this scheme. As noted previously, the method considered here for the creation of resources involves parallel production of many copies of a resource to ensure it is available on demand. This is a simple approach that leads to a higher cost in
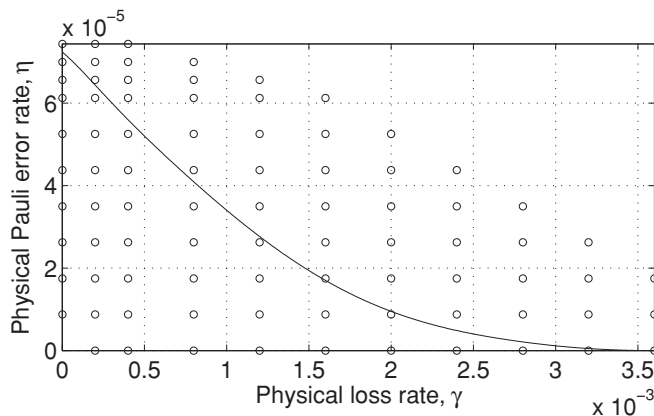

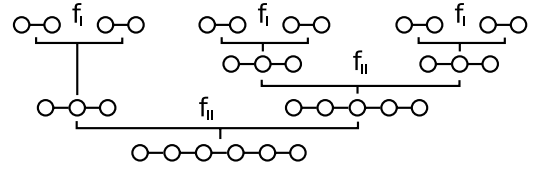FIG. 7. The threshold curve for optical parity-state computing using the 23-qubit GOLAY code.

FIG. 8. Process for generating a six-qubit parity state, beginning with six Bell states and performing two rounds of fusion gates.

terms of entangled photon generation and avoids more complicated resource-saving techniques such as storing previously prepared resources and "recycling" entangled states from unsuccessful attempts. Such techniques tend to require more intricate design and photon switching, as well as potentially introducing more errors due to the longer photon storage time.

We calculate the resources required in terms of the number of Bell states used. This a useful unit to consider as it is a common starting point for building entangled states across many optical schemes. It is also handy for comparisons with current optical quantum computation experiments as most use the entangled output of optical parametric down-conversion systems as photon sources.

As no recycling is used, the resource production has a 50% chance of failing for every fusion gate performed, meaning that the number of parallel attempts required doubles with each fusion gate. This exponential growth can be tolerated as it only occurs on a small scale—in our case none of the resource states need to be larger than eight qubits. To estimate the resources we calculate the average number of Bell states required to produce the appropriate resources using this parallel production method and implement a parity-encoded operation.

Much of this resource production simply involves the creation of ancillary parity states, which is done by linking the initial Bell states together using type I and II fusion gates (Fig. 8). State preparation at the parity layer requires a seven-qubit parity state, which would take an average of 448 Bell pairs to produce. Re-encoding, and hence the Z_{90} operation, would require an eight-qubit parity state for each attempt, and an average of two attempts to implement the operation. Hence we estimate the resources for the Z_{90} operation at 2048 Bell pairs on average. The circuit for the preparation of the XX'_{90} resource was shown previously in Fig. 3. This resource requires an average of 128 Bell pairs to produce.

As a basis for comparison, we will consider the requirements for producing the telecorrector state needed for one round of correction. Using the gate costs described above, it can be calculated that the state requires approximately 177,670 Bell pairs to generate. In Table I resource usage and threshold values are compared between parity-state and cluster-state schemes for optical quantum computing. Due to its greater difference from the other two schemes, we did not include in the table a scheme for quantum computing using "cat" states [7]. Cat states are in general more difficult to generate than Bell states, so this makes a direct comparison of resource usage difficult. We note that on average 10^3 cat states are needed to create a telecorrector state in that scheme. The loss threshold for the cat states is 2×10^{-4}, and a threshold for depolarization was not specified in that work.

Thus, our scheme for fault-tolerant parity-state quantum computing gives a resource usage figure three orders of

TABLE I. A comparison of thresholds and resource requirements for linear-optics quantum computing error correction schemes using a seven-qubit STEANE code. Here the resources are those required at threshold for the first level of telecorrection. The loss threshold given for each scheme is the maximum achievable in the case of no depolarization errors and vice versa.

Scheme	Loss threshold	Depolarization threshold	Resources
Cluster states	4×10^{-3}	8×10^{-5}	1.3×10^{8}[a]
Parity states	2×10^{-3}	2.4×10^{-5}	1.8×10^{5}

[a]Reference [6] quotes an incorrect resource usage number; the one cited here is the corrected value.

magnitude smaller than that for an equivalent cluster-state circuit [6] (and, in some sense, three orders of magnitude larger than the requirements for the cat-state version [7]). However, threshold is poorer than that of the cluster-state protocol but better (with respect to loss) than the scheme using cat states. Note that the scheme of Ref. [6] is just one example of many possible ways of designing a cluster-state error correction scheme, and it is conceivable that other cluster-state schemes would give quite different combinations of resource usage and threshold. It would be interesting to study whether such alternatives would follow a trade-off between resource usage and threshold in a way which is consistent with Table I.

VI. CONCLUSIONS

We have shown that an error-correcting system based on parity encoding falls in between other schemes in both threshold and resource requirements. The parity scheme has a higher error threshold than that found for cat states but also significantly larger resource requirements. Conversely, it is two orders of magnitude cheaper in resources than a cluster-state implementation when both schemes are operated at their thresholds but also has lower thresholds for both located and unlocated error rates. Together, these results suggest a necessary trade-off between resources and achievable threshold, which indicates that the preferred encoding method in any experimental attempt to demonstrate optical quantum error correction will depend on the capabilities and limitations of the physical system and its components.

It is worth noting the general principle demonstrated here: that concatenation can be used to tailor error correction to suit the relative error rates. In this case, some parity encoding is used to reduce the rate of failures due to nondeterministic gates to a level at which the remaining errors can be handled by the general error correction code. However, the same principle could be applied to other errors. For example, a system with a very high loss rate in comparison with other errors could use concatenation with a dedicated loss-correction code [13] to allow a higher threshold for loss at the cost of lower thresholds for other errors.

[1] E. Knill, R. Laflamme, and G. Milburn, Nature (London) **409**, 46 (2001).

[2] A. J. F. Hayes, A. Gilchrist, C. R. Myers, and T. C. Ralph, J. Opt. B: Quantum Semiclass. Opt. **6**, 533 (2004).

[3] D. E. Browne and T. Rudolph, Phys. Rev. Lett. **95**, 010501 (2005).

[4] A. Gilchrist, A. J. F. Hayes, and T. C. Ralph, Phys. Rev. A **75**, 052328 (2007).

[5] A. M. Steane, Phys. Rev. Lett. **77**, 793 (1996).

[6] C. M. Dawson, H. L. Haselgrove, and M. A. Nielsen, Phys. Rev. A **73**, 052306 (2006).

[7] A. P. Lund, T. C. Ralph, and H. L. Haselgrove, Phys. Rev. Lett. **100**, 030503 (2008).

[8] P. Kok, W. J. Munro, K. Nemoto, T. C. Ralph, J. P. Dowling, and G. J. Milburn, Rev. Mod. Phys. **79**, 135 (2007).

[9] T. B. Pittman, B. C. Jacobs, and J. D. Franson, Phys. Rev. A **71**, 052332 (2005).

[10] J. L. O'Brien, G. J. Pryde, A. G. White, and T. C. Ralph, Phys. Rev. A **71**, 060303 (2005).

[11] C. Lu, W. Gao, J. Zhang, X. Zhou, T. Yang, and J. Pan, Proc. Natl. Acad. Sci. USA **105**, 11050 (2008).

[12] S. Redner, *A Guide to First-Passage Processes* (Cambridge University Press, Cambridge, 2001).

[13] T. C. Ralph, A. J. F. Hayes, and A. Gilchrist, Phys. Rev. Lett. **95**, 100501 (2005).